Journal of Power Sources 195 (2010) 6504–6509

Contents lists available at ScienceDirect

Journal of Power Sources

journal homepage: www.elsevier.com/locate/jpowsour

Short communication

Influence of water vapor on performance of co-planar single chamber solid oxide fuel cells

Daehee Lee[a], Sung-Jin Ahn[a,1], Joosun Kim[b], Jooho Moon[a,*]

[a] Department of Materials Science and Engineering, Yonsei University, Seoul 120-749, Republic of Korea
[b] Nano-Materials Research Center, KIST, Seoul 136-791, Republic of Korea

ARTICLE INFO

Article history:
Received 2 February 2010
Received in revised form 23 March 2010
Accepted 29 March 2010
Available online 4 May 2010

Keywords:
Single chamber solid oxide fuel cell
Reaction mechanism
Water vapor
Impedance analysis

ABSTRACT

Influences of feeding gas compositions on the performance of co-planar, single chamber solid oxide fuel cells (SC-SOFCs) are investigated with emphasis on the role of water vapor. The maximum open circuit voltage (OCV) and peak power density are obtained at a methane-to-oxygen ratio of 3.5 under the wet gas condition, and a stoichiometric ratio of 2.0 for methane partial oxidation under the dry gas condition. In addition to the partial oxidation of methane on the anode and electrocatalytic reactions, both steam reforming and methane combustion occur on the anode and cathode, respectively, in the presence of water vapor. Local volume expansion and a rise in temperature associated with these parasitic reactions intensify inter-mixing of the reactant and product gases by which the OCV and power density drastically deteriorate with decreasing anode-to-cathode gap distance, as confirmed by impedance analysis for the LSM-YSZ|YSZ|LSM-YSZ symmetrical cell.

1. Introduction

The concept of single chamber solid oxide fuel cells (SC-SOFCs) remains fascinating to researchers because of its novel cell configuration that requires no gas-tight sealings between the anode and cathode, and direct utilization of hydrocarbon fuel without an external reformer. These characteristics provide several advantages over conventional SOFCs that make SC-SOFCs suitable for portable power generators, such as better mechanical and thermal shock resistances, thermal self-sustainability, less carbon deposition and system simplification [1]. Despite such merits, early research indicates that SC-SOFCs exhibit low electrochemical performance [2,3]. In recent years, however, there have been noticeable advances since their original description by Hibino et al. in 2002 [4]. More recently, Shao et al. [5] reported high performance for thermally self-sustainable SC-SOFCs with an open circuit voltage (OCV) of 1.44 V and a peak power density of 275 mW cm^{-2} at 600 °C.

For an ideal SC-SOFC, the operation mechanism is the same as for a conventional SOFC, which is based on the differences in catalytic activity of electrodes towards fuel and air. Both partial oxidation reactions of the hydrocarbon fuel and oxidation of hydrogen and carbon monoxide need to occur only at the anode, as described by:

$$C_nH_{n+2} + \frac{n}{2}O_2 \rightarrow \frac{(n+2)}{2}H_2 + nCO \quad (1)$$

$$H_2 + O^{2-} \rightarrow H_2O + 2e^- \quad (2)$$

$$CO + O^{2-} \rightarrow CO_2 + 2e^- \quad (3)$$

Alternatively, oxygen is reduced only at the cathode, as described by:

$$\frac{1}{2}O_2 + 2e^- \rightarrow O^{2-} \quad (4)$$

Ideally these selective oxidation and reduction reactions allow for differences in the oxygen partial pressure between the anode and cathode, which is a driving force for fuel cell operation [6]. As a result, the electromotive force between the two electrodes can be generated even when a mixed gas of fuel and air is used. However, under real operating conditions, the selectivity of electrodes towards partial oxidation of the fuel is insufficient to develop a maximum oxygen partial pressure gradient between the electrodes. A nickel-based anode would fully oxidize the fuel by heterogeneous catalytic reaction, and it may be itself oxidized in the SC-SOFC operation [7]. The $La_{0.8}Sr_{0.2}MnO_3$ (LSM) cathode could be reduced by reaction with methane, which results in a reduced electromotive force [8,9].

We have successfully developed new patterning methods for ceramic materials such as robo-dispensing and microfluidic lithography, for which the miniature co-planar SC-SOFCs with micropatterned interdigitated electrodes located on the side of the

* Corresponding author. Tel.: +82 2 2123 2855; fax: +82 2 365 5882.
E-mail address: jmoon@yonsei.ac.kr (J. Moon).
[1] Present address: Department of Mechanical Engineering, MIT, 77 Massachusetts Ave, Cambridge, MA 02139, United States.

0378-7753/$ – see front matter © 2010 Elsevier B.V. All rights reserved.
doi:10.1016/j.jpowsour.2010.03.101

electrolyte were readily fabricated [10–12]. However, the introduction of both a complex electrode geometry and mixed gas containing water vapor led to a decrease in the OCV and serious performance loss with decreasing electrode interspacing. This observation may have resulted from the reduced oxygen partial pressure gradient induced by inter-mixing of the reactant and product gases that occurs upon the undesirable exothermic parasitic reactions, however, a detailed mechanism and evidence that govern the temperature-rise and inter-mixing were not clearly elucidated. We speculate that such reductions in OCV and power density are attributed to methane steam reforming at the anode and catalytic combustion of methane at the cathode in addition to the partial oxidation of methane. Morel et al. reported the catalytic combustion of methane on the LSM cathode with methane-air mixture gas [13]. It was confirmed that the LSM cathode acts as a catalyst for full methane oxidation, i.e., combustion of methane. In this work, we investigated the influence of the parasitic reaction at the cathode on the performance of co-planar SC-SOFCs with complex electrode geometry depending upon the moisture of the gas mixture. The co-planar SC-SOFCs of NiO-YSZ|YSZ|LSM-YSZ with varying anode-to-cathode distances from 50, 75, to 100 μm were fabricated via microfluidic lithography techniques. OCVs, *I–V* characteristics and impedance spectra were investigated with and without water vapor.

2. Experimental

A co-planar SC-SOFC with interdigitated patterned electrodes was fabricated using yttria stabilized zirconia (YSZ, TZ8Y, Tosoh, Japan) as an electrolyte, LSM (Seimi, Japan)-YSZ as a composite cathode, and NiO (Sumitomo, Japan)-YSZ as a composite anode. YSZ powder was first compacted by uni-axial pressing under hydraulic pressure of 100 MPa followed by sintering at 1500 °C for 10 h. For the preparation of the anode cermet suspension, NiO and YSZ powders were mixed at a weight ratio of 50:50 and dispersed in ethanol with an appropriate dispersing agent by ball milling for 30 h. The solid loading of the anode suspension was 20 vol%. A cathode suspension mixture of LSM and YSZ was prepared at a weight ratio of 70:30 with a solid loading of 20 vol%.

The detailed procedure of microfluidic lithography was previously described [14]. An electrode master pattern was fabricated using conventional photolithography with a SU-8 50 photoresist (Microchem Corp., USA). A mixture of poly(dimethylsiloxane) (PDMS) prepolymer (Sylgard 184, Dow Corning Co.) was poured on the master pattern and cured at 80 °C for 1 h, resulting in a transparent elastomer mold with a surface relief pattern of interdigitated channels in an 5 mm × 5 mm area with electrode-to-electrode interspacing of 50, 75, and 100 μm. The elastomer was placed on the mirror polished surface of a YSZ disk electrolyte to produce a conformal contact. An anode suspension of 200 μL was dropped in a reservoir accessing the microchannel of the mold and then evacuated at 10 Torr in a vacuum chamber. Upon restoring to atmospheric pressure, the anode suspension was fully infiltrated into the microchannel by an induced pressure difference. After infiltration, the microfluidic device was dried at 24 °C overnight and the PDMS mold was peeled off from the electrolyte followed by sintering at 1350 °C for 1 h. Another PDMS mold was attached on the electrolyte containing the sintered anode pattern. Visual alignment between the micro-channel and patterned structure was achieved with an optical microscope (Leica DMLM). With the same technique as the anode fabrication, the cathode suspension was infiltrated and dried to form the cathode pattern, followed by sintering at 1100 °C for 1 h.

The resulting patterned SC-SOFCs were observed using confocal laser scanning microscopy (Olympus LEXT, Japan) and field emission scanning electron microscopy (FE-SEM, S-4200, Hitachi, Tokyo, Japan). After fabricating the SC-SOFCs, Au wires were attached to the ends of each patterned electrode with Au paste (ESL ElectroScience, PA, USA) and fired at 800 °C for 1 h. For the performance measurement, SC-SOFC cells on an alumina plate were placed in the middle of a quartz tube with a diameter of ~28 mm and a thermocouple was attached close to the cell. (Fig. 1) OCV and *I–V* characteristics of the SC-SOFCs were determined using a DC source meter (Keithley 2425) by current interruption method at 800 °C, while a mixture of nitrogen, methane, and oxygen was fed into the cell. A LSM-YSZ|YSZ|LSM-YSZ symmetrical cell was also prepared to study the influence of the water vapor on the performance by monitoring the electrochemical reaction activity near the cathode (Fig. 2). Electrochemical impedance measurements were performed using AC impedance spectroscopy (Solartron SI 1252/potentiostat 1287A) with or without 3 vol% water vapor.

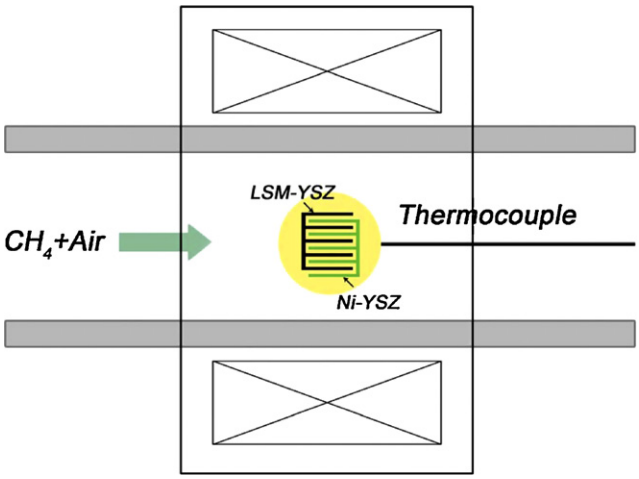

Fig. 1. Schematic presentations of the co-planar SC-SOFC measurement setup.

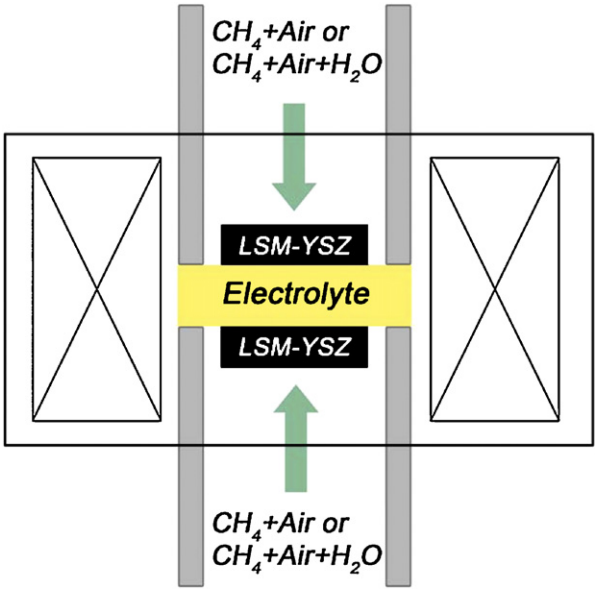

Fig. 2. Schematic presentations of the LSM-YSZ|YSZ|LSM-YSZ symmetrical cell for impedance analysis.

3. Results and discussion

Co-planar micro SC-SOFCs are successfully fabricated by microfluidic lithography. Fig. 3 shows 2-D and 3-D confocal laser

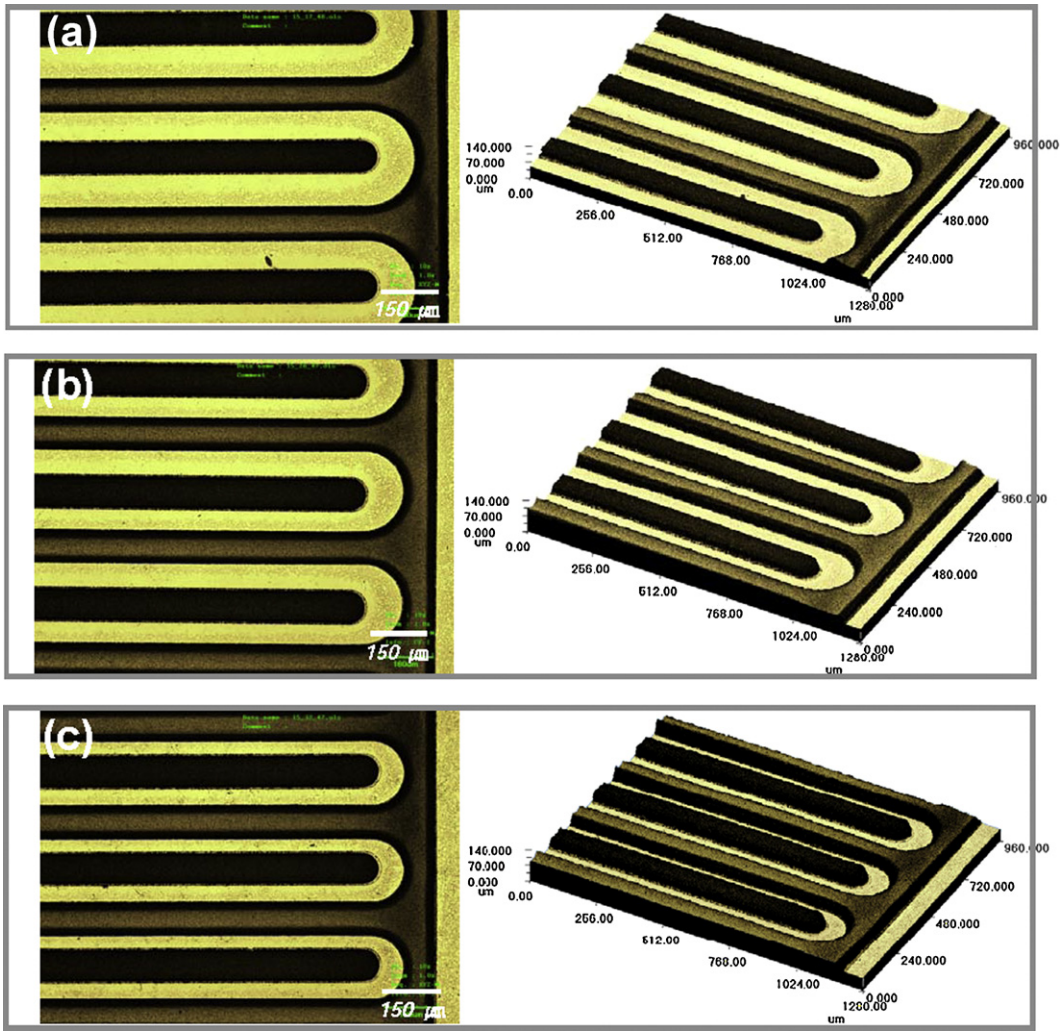

Fig. 3. Two and three-dimensional laser confocal microscopic images of the fabricated co-planar SC-SOFCs with interdigitated electrodes that have (a)/(b) 100 μm, (c)/(d) 75 μm, and (e)/(f) 50 μm anode-to-cathode distance.

scanning images of the fabricated 5 mm × 5 mm SC-SOFC with an electrode width of 100 μm, thickness of 45 μm, and anode-to-cathode distance of 50, 75, and 100 μm. Patterned electrodes consisting of 16 pairs of anodes and cathodes exhibit well-defined edge features without any defects even though they have a complex geometry and a high aspect ratio. SEM images of the sintered anode and cathode microstructures are shown in Fig. 4. Both electrode microstructures are relatively denser than those of the conventional SOFC electrodes which have a typical porosity greater than ~30%. The dense structure originates from the unique drying mechanism involved in microfluidic lithography [14], which requires the pore formers to optimize the microstructure of the electrodes.

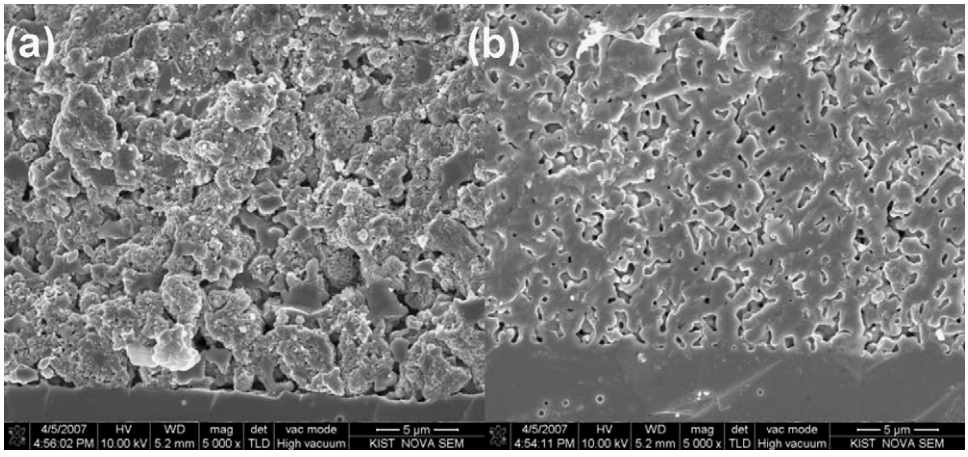

Fig. 4. Cross-sectional SEM images of dense (a) anode and (b) cathode microstructures produced by microfluidic lithography after sintering at 1350 and 1100 °C, respectively.

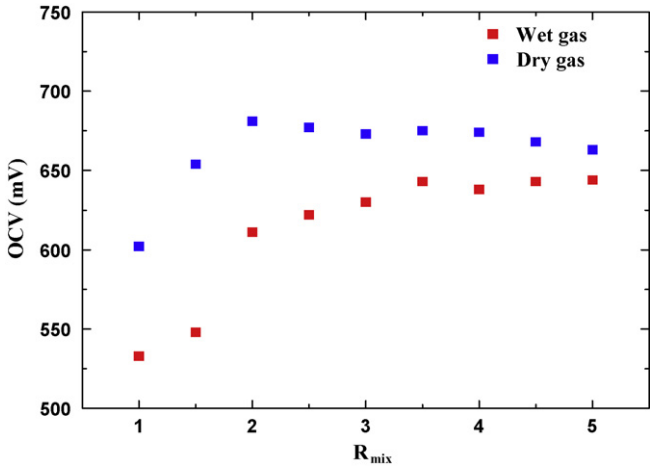

Fig. 5. OCV variation of the co-planar SC-SOFCs with interdigitated electrode structures and the anode-to-cathode distance of 100 μm at 800 °C, while varying the methane-to-oxygen ratio (R_{mix}) from 1.0 to 4.0 with or without 3 vol% water vapor.

The feeding gas composition plays an important role in determining the cell performance, especially for co-planar SC-SOFCs [15]. The fuel-to-oxygen mixing ratio needs to be controlled to assure the partial oxidation of the fuel on the anode, avoiding parasitic reactions such as carbon coking and combustion of fuel [16,17]. Local temperature rise induced by exothermic anode reactions and the complex electrode geometry would cause the inter-mixing of the reactant and product gases, which in turn decreases the oxygen partial pressure gradient between the anode and cathode. The water vapor may also induce the steam reforming of fuel and the catalytic combustion of fuel. Here we evaluate the influences of gas composition and water vapor on the OCV value for cells with an anode-to-cathode distance of 100 μm, as shown in Fig. 5. Mixed gas with varying molar ratios of methane to oxygen (R_{mix}) is fed to the cells, while the total flow rate is fixed to 120 sccm when dry gas is used and 210 sccm when wet gas is used, so that the amounts of the oxygen flow are kept constant in both wet and dry conditions. The presence of water vapor causes differences in dependence of R_{mix} on the OCV. In the case of dry gas, the maximum OCV is 681 mV when the stoichiometric value for methane partial oxidation is $R_{mix} = 2.0$ (Eq. (5)) [15].

$$CH_4 + \tfrac{1}{2}O_2 \rightarrow 2H_2 + CO \quad \Delta H^0_{298\,K} = 35.6\,kJ\,mol^{-1} \tag{5}$$

In contrast, in the case of wet gas, a maximum OCV value of 648 mV is observed at $R_{mix} \geq 3.0$. Similar tendencies are observed with the *I–V* characteristics. The R_{mix} value also has an influence on the power output of SC-SOFCs and the maximum power density is obtained at $R_{mix} = 2.0$ for dry gas and $R_{mix} = 3.5$ for wet gas. A higher R_{mix} is needed for the maximum performance under the wet gas condition due to the steam reforming reaction (Eq. (6)) that consumes methane, requiring additional fuel supply:

$$CH_4 + H_2O \rightarrow 3H_2 + CO \quad \Delta H^0_{298\,K} = 206\,kJ\,mol^{-1} \tag{6}$$

Furthermore, the obtained maximum OCV is lower than the theoretical value derived from the Nernst equation, which is due to a relatively lower total mixed gas flow rate of 120–210 sccm. It has been reported that increasing the mixture gas flow rate improves OCV as well as the performance of the cell [18,19].

Fig. 6 shows the performance of the co-planar SC-SOFCs with interdigitated electrodes while varying the anode-to-cathode distance under either dry or wet gas conditions at 800 °C. As summarized in Table 1, OCVs for these SC-SOFCs largely decrease from 643, 543, to 470 mV under the wet gas condition with decreasing anode-to-cathode distance of 100, 75, and 50 μm, respectively

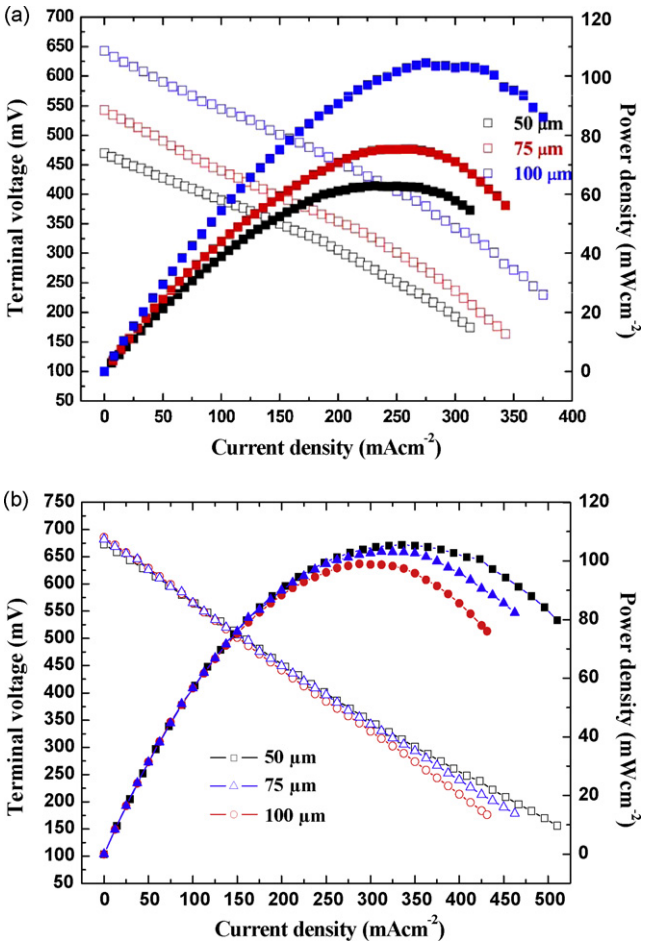

Fig. 6. *I–V* characteristics of co-planar SC-SOFCs with an interdigitated electrode pattern and varying anode-to-cathode distances of 50, 75, and 100 μm at 800 °C flowing mixed gas of (a) 60 sccm CH_4 + 16 sccm O_2 + 64 sccm N_2 containing 3% H_2O ($R_{mix} = 3.5$), and (b) 60 sccm CH_4 + 30 sccm O_2 + 120 sccm N_2 without vapor ($R_{mix} = 2.0$).

(Fig. 6a), whereas small OCV drops from 686, 682, to 672 mV are observed under the dry gas condition (Fig. 6b). Increasing the anode-to-cathode distance deteriorates the cell power density due to the increased ohmic resistance as indicated by a gradual increase in the slope of the *I–V* curve under the dry gas condition. The inter-electrode gap distance also controls the OCV of co-planar SC-SOFCs, but its influence depends on the water vapor content of the mixed gas. Decreases from the theoretically calculated OCV can be attributed to the inter-mixing of the reactant and product gases induced by exothermic electrode reactions, which reduces the oxygen partial pressure difference between the electrodes. Partial oxidation of the methane on the anode is always accompanied by heat evolution such that the anode has a higher local temperature than the cathode. The local temperature gradient across the electrodes would induce both the convection flow and mass transport by which the product gases at the anode are transferred toward the cathode [20]. Narrowing the inter-electrode gap would intensify the variation of local gas composition by the inter-mixing of the reactant and product gases. However, less dependence of OCV on the inter-electrode gap distance observed in Fig. 6b indicates that the inter-mixing is insignificant under the dry gas condition.

Inter-mixing of the reactant and product gases is enhanced when water vapor is introduced in the mixed gas. As previously mentioned, the presence of water vapor may cause steam to reform. In spite of its endothermic nature, steam reforming involves a larger volume expansion due to the increased number of moles (Eq. (6))

Table 1
Dimensions of SC-SOFCs fabricated via microfluidic lithography and the corresponding electrical performance as a function of the anode-to-cathode gap distance and water vapor.

Anode-to-cathode distance		100 μm	75 μm	50 μm
Wet gas	OCV (mV)	643	543	470
	Power density (mW cm^{-2})	104	75	63
Dry gas	OCV (mV)	686	682	672
	Power density (mW cm^{-2})	99	103	105

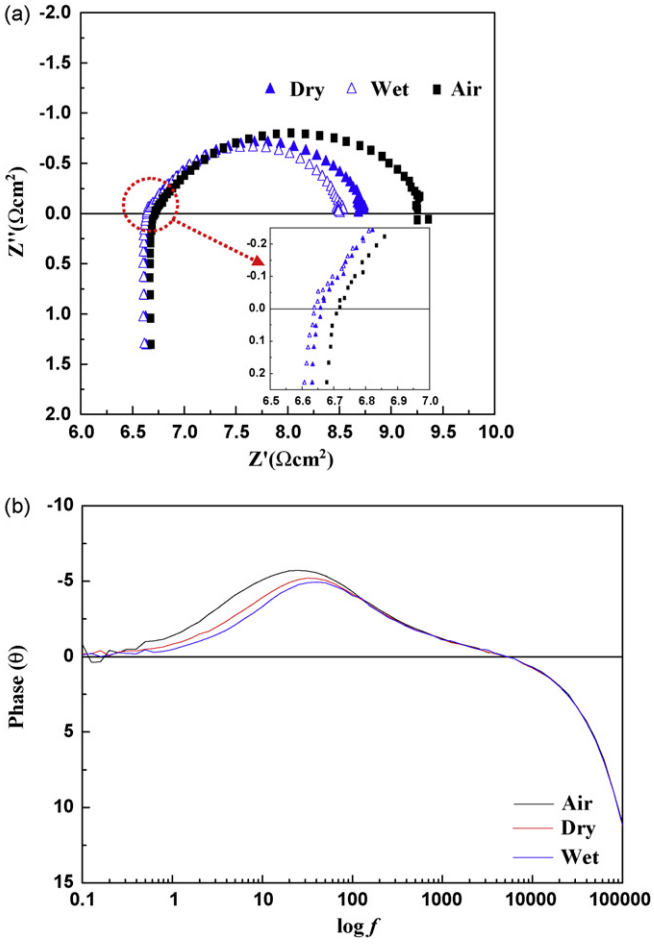

Fig. 7. (a) Impedance spectra of the LSM-YSZ|YSZ|LSM-YSZ symmetrical cell with 80 sccm N_2 + 20 sccm O_2 (Air), 40 sccm CH_4 + 20 sccm O_2 + 80 sccm N_2 (dry), and 40 sccm CH_4 + 20 sccm O_2 + 80 sccm N_2 containing 3% water vapor (wet); (b) Bode plots of impedance spectra as a function of the feeding gas conditions.

as compared to the partial oxidation of methane (Eq. (5)), which can mix the reactant gas with the product gas. In addition, the LSM cathode can play a role as a methane combustion catalyst at high temperatures [13]. Methane combustion expressed in Eq. (7) would cause a drastic increase in local temperature near the cathode as it is a stronger exothermic reaction than the partial oxidation of methane at the anode:

$$CH_4 + 2O_2 \rightarrow 2H_2O + CO_2 \quad \Delta H^0_{298\,K} = -889\,kJ\,mol^{-1} \tag{7}$$

Such a temperature increase will improve ionic conduction and surface diffusion in both the electrode and electrolyte. Alternatively, the consumption of oxygen near the cathode by methane combustion would pose a kinetic penalty toward the cathode reaction (i.e., an increase in the cathodic polarization resistance) as well as decrease the oxygen partial pressure gradient between the anode and cathode.

Fig. 7a shows the impedance spectra of the LSM-YSZ|YSZ|LSM-YSZ symmetrical cell under different feeding gas conditions. High frequency intercepts of the spectra, which represent the ohmic resistance of the cell, are diminished as the methane-air mixture gas is fed instead of air, and the additional decrease is detected when water vapor is added indicating an increase in cell temperature. If the presence of water permits methane oxidation on the cathode, oxygen consumption would lead to an increase in total polarization resistance. On the contrary, the total polarization resistance is reduced, indicative of thermal activation of the electrochemical oxygen reduction. This observation supports that a significant temperature-rise generated by methane combustion overwhelmed the influences of the diminished oxygen partial pressure gradient and the polarization resistance increase by oxygen depletion. As shown in Fig. 7b, Bode plots also shows the decrease in the capacitance as the methane-air mixture gas is fed instead of air, and further decrease is observed when water vapor is present, indicating fast conversion of oxygen gas to ions. These findings clearly suggest that the LSM cathode catalyzes the full oxidation of methane, accompanying a significant rise of the cell temperature in the presence of the water vapor. Greater heat evolution associated with the methane combustion produces a temperature gradient between the electrodes as compared to heat involved in the partial oxidation of methane, causing the inter-mixing of the reactant and product gases and reducing the oxygen potential gradient. Narrowing the inter-electrode gap distance intensifies the inter-mixing and decreases the OCV, as shown in Fig. 6a. The deteriorated cell power density under the wet gas condition results from the OCV loss due to the extensive inter-mixing (see Table 1). The cell with a 100 μm inter-electrode gap distance has a steeper slope in the *I–V* curve than the cells of 50 μm, indicative of larger activation and ohmic losses. This demonstrates that the actual local temperature of the 100 μm-spaced cell would be less than that associated with the 50 μm-spaced cell because the heat evolution effect by methane combustion is less significant in the larger spaced electrode structures.

4. Conclusions

We investigate the influence of the feeding gas composition on the performance of co-planar SC-SOFCs with varying anode-to-cathode distances and interdigitated electrodes. The fuel-to-oxygen mixing ratio is controlled to ensure high performance. Maximum OCV and power density are obtained at 800 °C when using a mixed gas ratio of R_{mix} = 2.0 under the dry gas condition, whereas R_{mix} = 3.5 is optimal under the wet gas condition. The presence of water vapor allows for two parasitic reactions on each electrode in addition to the partial oxidation of methane and the electrocatalytic reactions. Steam reforming that involves larger volume expansion occurs on the anode to consume the methane, whereas the methane combustion that includes greater heat evolution occurs on the cathode along with oxygen consumption. Such local volume expansion and temperature-rise would induce both the convection flow and mass transport by which the reactant gas is inter-mixed with the product gas. This inter-mixing prevents the cells from developing the maximum oxygen partial pressure

gradient between the anode and cathode, deviating the OCV from the Nernst equation. Narrowing the inter-electrode gap intensifies the inter-mixing, which significantly deteriorates the OCV and power density. The presence of parasitic reactions is confirmed by impedance analysis of the LSM-YSZ|YSZ|LSM-YSZ symmetrical cell under different feeding gas conditions. These results provide an in-depth understanding of the role of water vapor and how it critically governs the performance of SC-SOFCs.

Acknowledgements

This work was supported by the National Research Foundation (NRF) funded by the Ministry of Education, Science and Technology (2007-313-D00338 and 2009-0093454). It was also partially supported by the Second Stage of the Brain Korea 21 Project.

References

[1] T. Hibino, A. Hashimoto, T. Inoue, J. Tokuno, S. Yoshida, M. Sano, Science 288 (2000) 2031–2033.
[2] T. Hibino, H. Iwahara, Chem. Lett. 7 (1993) 1131–1134.
[3] T. Hibino, Y. Kuwahara, S. Wang, J. Electrochem. Soc. 146 (1999) 2821–2826.
[4] T. Hibino, A. Hashimoto, M. Yano, M. Suzuki, S. Yoshida, M. Sano, J. Electrochem. Soc. 149 (2002) A133–A136.
[5] Z. Shao, S.M. Haile, J. Ahn, P.D. Ronney, Z. Zhan, S.A. Barnett, Nature 435 (2005) 795–798.
[6] I. Riess, P.J. van der Put, J. Schoonman, Solid State Ionics 82 (1995) 1–4.
[7] X. Jacques-Bédard, T.W. Napporn, R. Roberge, M. Meunier, J. Power Sources 153 (2006) 108–113.
[8] I. Riess, J. Power Sources 175 (2008) 325–337.
[9] M. Yano, A. Tomita, M. Sano, T. Hibino, Solid State Ionics 177 (2007) 3351–3359.
[10] S.-J. Ahn, J.-H. Lee, J. Kim, J. Moon, Electrochem. Solid-State Lett. 9 (2006) A228–A231.
[11] S.-J. Ahn, Y.-B. Kim, J. Moon, J.-H. Lee, J. Kim, J. Electroceram. 17 (2006) 689–693.
[12] S.-J. Ahn, Y.-B. Kim, J. Moon, J.-H. Lee, J. Kim, J. Power Sources 171 (2007) 511–516.
[13] B. Morel, R. Roberge, S. Savoie, T.W. Napporn, M. Meuiner, Appl. Catal. A: Gen. 323 (2007) 181–187.
[14] S.-J. Ahn, J. Moon, J. Am. Ceram. Soc. 88 (2005) 1171–1174.
[15] T.W. Napporn, X.J. Bedard, F. Morin, M. Meunier, J. Electrochem. Soc. 151 (2004) A2088–A2094.
[16] T. Ishihara, Y. Takita, Catal. Surv. Japan 4 (2001) 125–133.
[17] V.R. Choudhary, V.H. Rane, A.M. Rajput, Catal. Lett. 22 (1993) 289–297.
[18] I.C. Stefan, C.P. Jacobson, J. Visco, L.C. De Jonghe, Electrochem. Solid-State Lett. 7 (2004) A198–A200.
[19] T. Suzuki, P. Jasinski, V. Petrovsky, H.U. Anderson, F. Dogan, J. Electrochem. Soc. 152 (2005) A527–A531.
[20] T.W. Napporn, F. Morin, M. Meunier, Electochem. Solid-State Lett. 7 (2004) A60–A62.